First-principle-based full-dispersion Monte Carlo simulation of the anisotropic phonon transport in the wurtzite GaN thin film

Ruikang Wu, Run Hu,[a] and Xiaobing Luo[a]
State Key Laboratory of Coal Combustion and Thermal Packaging Laboratory, School of Energy and Power Engineering, Huazhong University of Science and Technology, Wuhan 430074, China

(Received 28 January 2016; accepted 29 March 2016; published online 13 April 2016)

In this study, we developed a first-principle-based full-dispersion Monte Carlo simulation method to study the anisotropic phonon transport in wurtzite GaN thin film. The input data of thermal properties in MC simulations were calculated based on the first-principle method. The anisotropy of thermal conductivity in bulk wurtzite GaN is found to be strengthened by isotopic scatterings and reduced temperature, and the anisotropy reaches 40.08% for natural bulk GaN at 100 K. With the GaN thin film thickness decreasing, the anisotropy of the out-of-plane thermal conductivity is heavily reduced due to both the ballistic transport and the less importance of the low-frequency phonons with anisotropic group velocities. On the contrary, it is observed that the in-plane thermal conductivity anisotropy of the GaN thin film is strengthened by reducing the film thickness. And the anisotropy reaches 35.63% when the natural GaN thin film thickness reduces to 50 nm at 300 K with the degree of specularity being zero. The anisotropy is also improved by increasing the surface roughness of the GaN thin film. © *2016 AIP Publishing LLC*.
[http://dx.doi.org/10.1063/1.4945776]

I. INTRODUCTION

With the dimension of electronic devices approaching nanometer scale, efficient heat removal is of great importance to their performances and functions. Due to its superior electronic, thermal, and optoelectronic properties, gallium nitride (GaN) with a broad band gap of 3.4 eV is widely used in microelectronic and optoelectronic devices such as laser diodes and light-emitting diodes (LEDs).[1–5] As an important material in GaN-based LED chips, thermal properties of the wurtzite GaN make a huge difference in LED performances. It is known that the main heat carriers in semiconductors are the quanta of energy called phonons generated by the lattice vibration, rather than electron-hole pairs. Therefore, the phonon transport dominates the heat transfer in LED chips. However, GaN layers in LED chips may have the film thickness less than 100 nm,[6] much smaller than the phonon mean free path (MFP) in GaN at 300 K;[7] thus, strong size effect may exist. Besides, the wurtzite GaN has a hexagonal wurtzite lattice structure which is not isotropic and the thermal conductivity anisotropy of GaN was rarely studied. Thereby, the study of anisotropic thermal properties in the wurtzite GaN thin film is extremely required.

Experiments on the thermal transport investigation with finite size effect in nanometer scale are very hard to handle and measure, relative to which the theoretical predictions seem essential. MC simulation, which has the advantages of simulating within a large range of dimension from several nanometers to micron sizes with low computational cost, is an appropriate method to study the thermal transport in thin films of realistic devices under the phonon level. The method has been applied to study the phonon transport in silicon, germanium, GaN, and other materials successfully.[8–14] Mazumder and Majumdar presented a comprehensive MC method accounting for dual polarizations of phonon propagation and non-linear relationships,[15] but optical phonons were not included[16,17] and phonons were generated isotropically into the simulation zone. Following researches were generally based on this method. However, in the method presented by Mazumder and Majumdar, only partial phonon dispersion relationships were considered, the isotropic hypothesis was introduced, and the scattering rates were usually achieved by semi-empirical formulas. Mei *et al.* presented a full-dispersion MC simulation method accounting for all three acoustic phonon branches to study the phonon transport in micron-sized graphene nanoribbons.[18] Inspired by this work, if the anisotropic properties of wurtzite GaN thin film are studied, it is required to take all the phonon modes and properties into account, since the anisotropy is reflected by phonon states in the MC method. On the other hand, accurate anharmonic properties and the full-dispersion relation can be obtained by using the first principle method based on density-functional perturbation theory (DFPT) by calculating the third-order interatomic force constants (IFCs).[19] Lindsay *et al.*[20] calculated the thermal conductivity of GaN using first principles and got the value of 242 W/mK at 300 K with naturally occurring Ga isotope concentrations (natural GaN), in agreement with measured room temperature values around 230 W/mK.[21] However, the first principle method has a great accuracy but with a huge computational cost, so it is limited to investigate systems within several nanometers.

From the comparison of MC and first-principle method, the advantages of each method are obvious and appealing. Could we combine these two methods together to make the best of these advantages (high accuracy and large computational size range) simultaneously? If so, the combined

[a]Electronic addresses: hurun@hust.edu.cn and luoxb@hust.edu.cn

method must have more extensive applications from nanometer scale to micron scale with enough accuracy. To explore the exact answer of this question is the right motivation behind this study.

In this study, we proposed an improved full-dispersion MC simulation method coupled with the first-principle method. The first principle method is applied to calculate the phonon dispersion relation as well as scattering rates of intrinsic and isotopic scatterings just for once. The input phonon states for the MC calculation, including the full-dispersion relation and anharmonic properties, all come from the first principle calculation. The anisotropy of the thermal conductivity in the bulk GaN, and along the in-plane and out-of-plane directions in GaN film, is discussed and analyzed in detail. The paper is organized as follows. In Section II, we present the algorithm for the first-principle-based full-dispersion Monte Carlo (FMC) simulation method. In Section III, we analyze the anisotropy of the thermal conductivity in the bulk GaN (Section III A), the anisotropy properties of the out-of-plane direction in the GaN thin film (Section III B), and the anisotropy of the phonon transport of the in-plane direction in the GaN thin film (Section III C). Finally, we conclude the whole study in Section IV.

II. FULL-DISPERSION MONTE CARLO METHOD

Phonons can be treated as semi-classical particles when the system characteristic size is comparable with the phonon MFP. MC method solves the Boltzmann transport equation (BTE) through tracking the phonon drift and interactions. When phonons are generated into the simulation zone, they travel through space, have interactions with geometry boundaries, and engage in scattering processes with phonons (intrinsic scattering), isotope defects (isotopic scattering), electrons, dislocations, and grain boundaries. However, we only considered the intrinsic and isotopic scatterings in this article, which are the main scattering mechanisms. Phonon properties including location, group velocity, frequency, polarization, anharmonic, and isotopic scattering rates should be initialized at the beginning of the MC method. In this section, we present our approach to obtain initial phonon properties from first principle calculation and apply the calculated results into FMC method. Other details of the MC simulation method can be found in previous works.[15,18,22–24]

A. First principle calculation

The first principle calculation of thermal conductivity has been developed by combining accurate calculations of the harmonic and anharmonic interatomic force constants using density functional theory (DFT) and DFPT with the solution of BTE. Recently, Li *et al.* published an open-source code ShengBTE,[25] which is available to calculate the third-order IFCs using a real-space finite-difference approach.[20] The real-space supercell approach to anharmonic IFC calculations is implemented by a script, thirdorder.py.[25] However, in order to run the thirdorder.py script, the harmonic IFCs calculated by the QUANTUM ESPREESO package[26] are required. All the expected values of the wurtzite GaN are calculated using norm-conserving pseudopotentials in the Perdew-Wang local density approximation (LDA).

We set the converged lattice constants of the wurtzite GaN to be $a = 3.166$ Å, $c = 5.124$ Å, and $u = 0.376$. These values, which are in good agreement with experimentally determined values,[27] $a_{exp} = 3.190$ Å, $c_{exp} = 5.189$ Å, and $u_{exp} = 0.377$, were obtained by optimizing the lattice structure with the chosen pseudopotentials using the QUANTUM ESPREESO package. A $4 \times 4 \times 2$ supercell was employed for second-order calculations and the phonon dispersion calculated from the harmonic IFCs along several high-symmetry directions for wurtzite GaN is shown in Fig. 1. It can be seen that the calculated phonon dispersion curves are in good agreement with the experimental data.[28,29] We also employed a $4 \times 4 \times 2$ supercell containing 128 atoms for anharmonic calculations and only the interactions up to seventh nearest neighbors were considered. Thermal conductivities along x, y, z directions of the lattice, namely, $[01\bar{1}0]$, $[2\bar{1}\bar{1}0]$, and $[0001]$ directions, respectively, are obtained using the ShengBTE package.

B. Phonon state determination

The third-order anharmonic calculation of wurtzite GaN was performed with $32 \times 32 \times 32$ **q**-point grids, generating 32768 discrete **q**-points in the reciprocal space and the phonon frequencies at each **q**-point. Due to the fact that four atoms exist in a primitive cell, there are three acoustic and nine optical phonon branches, corresponding to 12 phonon frequencies for each **q**-point.

Using the data of 32768 discrete points directly as the input data of the MC method would lead to immensely computational cost. Fortunately, the ShengBTE package calculated results contain a trail of files including phonon properties of frequencies, group velocities, anharmonic, and isotopic scattering rates of the irreducible unit cell in the first Brillouin zone. The irreducible unit cell only consists of 1734 discrete points in the reciprocal space. According to the symmetric

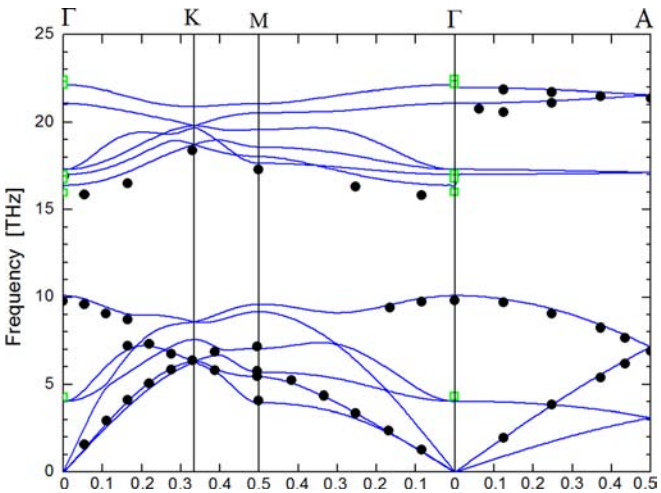

FIG. 1. Calculated phonon dispersion of wurtzite GaN along several high-symmetry directions. The solid lines are the results of our first principle calculation. The filled circles are the measured phonon frequencies by inelastic x-ray scattering from Ref. 28. The hollow diamonds at $\bar{q} = 0$ show the Raman scattering data from Ref. 29.

properties of the wurtzite GaN lattice structure, each discrete irreducible point represents a series of phonons with the same phonon properties except for group velocities. The degenerate schematic diagram of the *x*-*y* plane in the reciprocal space is shown in Fig. 2. All the points with index "a" and "b" are the equivalent corresponding reducible points due to twelve symmetric axes in the *x*-*y* plane, respectively. The irreducible part of 1734 discrete points is the shaded triangle in the schematic diagram. Phonon states can be initiated by using the irreducible information and the group velocity initiation will be discussed in Section II C.

Phonons are created under thermodynamic equilibrium with the local temperature T. The equilibrium phonon distribution function is given by the Bose-Einstein distribution, as

$$f^{eq}(\omega,p,T)=\frac{1}{\exp(\hbar\omega/k_BT)-1}, \tag{1}$$

where $\hbar$ is the reduced Planck constant, k_B is the Boltzmann constant, and p represents the polarization branch. The phonon frequency must be determined before the initiation. Firstly, we select the irreducible point that has the corresponding phonon state and then determine the phonon branch at this point. The cumulative energy density function of the irreducible discrete points can be expressed as

$$F_i=\sum_{j=1}^{i}\sum_{p}E_j(\omega,p)\Big/\sum_{j=1}^{N_{ir}}\sum_{p}E_j(\omega,p), \tag{2}$$

with

$$E_j(\omega,p)=\hbar\omega_{j,p}[f^{eq}(\omega_{j,p},p,T)-f^{eq}(\omega_{j,p},p,T_{ref})]\times G_j/(N_{all}V), \tag{3}$$

where N_{ir} is the number of irreducible points, N_{all} is the number of all the discrete **q**-points, T_{ref} is the selected reference temperature, V is the volume of the primitive cell, and G_j is the weighting factor, i.e., the total number of the equivalent **q**-points corresponding to the jth irreducible point. Then, a random number R_q is generated to decide which **q**-point should be selected. If $F_{i-1}<R_q\le F_i$ is satisfied, we select the i th **q**-point. The polarization probabilities should be determined by computing the ratio of the phonon energy of each polarization branch to the total phonon energy at the ith **q**-point

$$P_{i,p_j}=\sum_{k=1}^{j}E_i(\omega_{i,p_j},p_j)\Big/\sum_{k=1}^{12}E_i(\omega_{i,p_j},p_j). \tag{4}$$

Therefore, the phonon frequency ω_{i,p_j} is initialized and the phonon state is correlated with the jth polarization branch of the ith irreducible **q**-point. Thus, the phonon state data in the series of first principle output data files can be located. It has to be noticed that the polarization in this article is only used to locate the phonon state in the first principle output data.

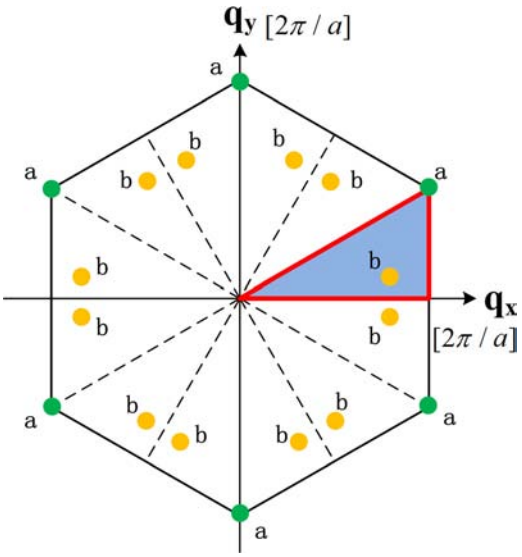

FIG. 2. The degenerate schematic diagram of the x-y plane in the first Brillouin zone. Points with index "a" and "b" are different groups of irreducible points owing to twelve symmetric axes. The shaded triangle is one of the twelve equivalent irreducible regions.

C. Phonon generation

Isothermal boundaries emit phonons under thermodynamic equilibrium at the boundary temperature into the simulation domain. As the anisotropy is taken into account, a phonon should have a certain initial group velocity. The ShengBTE package calculates three dimensional group velocities, v_{xl}, v_{yl}, v_{zl}, at each **q**-point for lattice directions of $[01\bar{1}0]$, $[2\bar{1}\bar{1}0]$, and [0001], respectively (under the lattice coordinate system).

We consider two different kinds of wurtzite GaN thin films with respect to various lattice directions as shown in Fig. 3. We call the situation that the lattice direction [0001] is along the thin film thickness direction as *C*-mode and the lattice direction $[01\bar{1}0]$ along the thin film thickness direction as *A*-mode. Under the *C*-mode condition, the phonon group velocity should be assigned to be $v_x=v_{zl}$, $v_y=v_{yl}$, and $v_z=v_{xl}$ due to the coordinate system exchange as shown in Fig. 3. v_x, v_y, and v_z are the three components of phonon group velocities under the coordinate system defined in the GaN thin film model, which is different from the lattice coordinate system as shown at the top left of Fig. 3; i.e., the z-component phonon velocity obtained from the first principle, which is along the film thickness direction of the GaN thin film under the *C*-mode condition, should be transformed to v_x to fit the coordinate system of the model. However, the coordinate system does not need to change in the *A*-mode.

In the MC simulation, particles are generated representing groups of phonons with similar properties.[22] Each particle can have different number of phonons but carry the same effective energy, given as

$$\varepsilon_{eff}^{d}=\frac{(L_xL_yL_z)\sum_{j=1}^{N_{ir}}\sum_{p}E_j(\omega,p)}{N_{in}}, \tag{5}$$

where N_{in} is the number of particles expected to be generated into the system within each time step. The number of

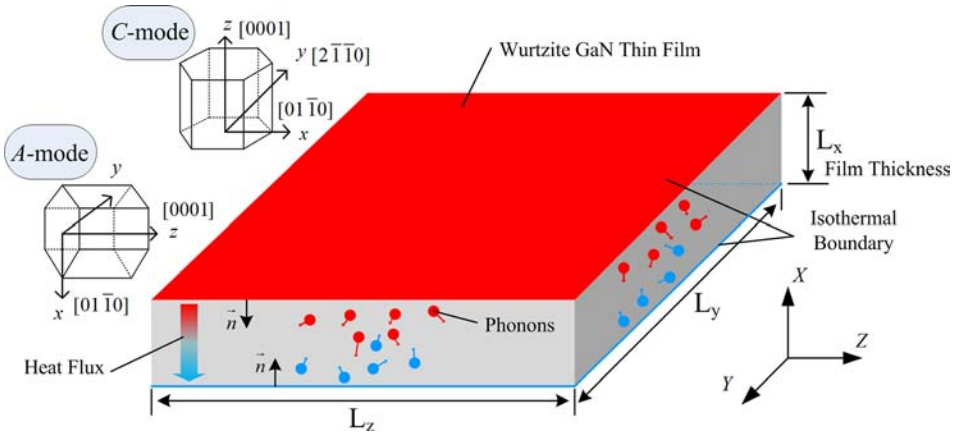

FIG. 3. A sketch map of two different kinds of wurtzite GaN thin film simulation domains with two different lattice directions along the thin film thickness direction. The coordinate system of the thin film is presented in the lower right corner.

particles emitted from a boundary face of the area (L_yL_z) and the boundary temperature T_b is given as

$$N_b = \frac{(L_yL_z)\Delta t}{(N_{all}V)\varepsilon_{eff}^d}\sum_{j=1}^{N_{ir}}\sum_{p}\hbar\omega_{j,p}\cdot\left|f^{eq}(\omega_{j,p},p,T_b) - f^{eq}(\omega_{j,p},p,T_{ref})\right|\cdot\left|\sum v_{x,j,in}\right|, \quad (6)$$

where $v_{x,j,in}$ is the x component of the generated phonon group velocity corresponding to the jth irreducible $\mathbf{q}$-point and should be satisfied by $\vec{v}_{g,j,in}\cdot\vec{n} > 0$, where $\vec{v}_{g,j,in}$ is the group velocity and $\vec{n}$ is the unit normal vector of the isothermal boundary which points into the simulation domain, as shown in Fig. 3. As the simulation domain is on one side of an isothermal boundary, we only calculate phonons that are able to be emitted into the simulation system, which means only half-side group velocities are initialized at each isothermal boundary.

D. Phonon scattering

We treated the phonon-boundary interaction as phonon reflection which is explicitly taken care of during the drift process. These boundaries are treated as adiabatic walls or partially specular reflectors, depending on the degree of specularity d. If d is set to be unit, then phonons are specularly reflected, implying that this boundary is treated as the periodic boundary condition. Otherwise, phonons might be reflected diffusely by a boundary with d less than unit.

Phonons' intrinsic and isotopic scattering rates can be easily initialized from the first principle results once the phonon frequencies are determined. The probability of scattering after time step Δt is[30]

$$P_{scattering}(\omega,p) = 1 - \exp(-\Delta t\cdot\tau_{total}^{-1}(\omega,p)), \quad (7)$$

where $\tau_{total}^{-1} = \tau_{3ph}^{-1} + \tau_i^{-1}$. τ_{3ph}^{-1} and τ_i^{-1} are three-phonon and isotopic scattering rates, respectively. Then, a random number R_s is created to decide whether the phonon scatters or not after the time step Δt. If $R_s > P_{scattering}$, the phonon scattering event occurs. Then, we should figure out which kind of scattering process it is by generating another random number, according to the relative scattering probability given as

$$P_k = \tau_k^{-1}/\tau_{total}^{-1}, \quad (8)$$

where the index k represents the category of different scattering mechanisms. As intrinsic scatterings help to rebuild the equilibrium, phonon states are redistributed from equilibrium distribution at the local temperature. The local temperature may be different from the temperature corresponding to the first principle calculated data, but the error can be neglected if the temperature discrepancies are small enough. In this article, the maximum temperature difference in the simulation domain is assigned to be 10 K. The phonon states' redistribution is performed by deleting the scattered phonons and generating new phonons from the equilibrium distribution. However, the generated group velocities are not limited by emitting direction that is only considered under the isothermal boundary emitting condition. In isotopic scattering processes, phonon properties remain unchanged except for phonon group velocity directions. Since phonons are just diffusely reflected by isotopes, in the isotopic scattering mechanism, new phonon group velocities are assigned isotropically.

III. RESULTS AND DISCUSSION

A. Anisotropy in bulk GaN

We calculated thermal properties for isotopically pure GaN and naturally occurring Ga isotopic GaN. The thermal conductivity of the bulk GaN between 100 K and 500 K is obtained through anharmonic calculations and the results are shown in Fig. 4. The first-principle calculated thermal conductivity for natural GaN is in good agreement with experiment values measured by Slack *et al.*[31] In addition, the isotropic thermal conductivity for natural GaN calculated by $(k_x + k_y + k_z)/3$, which is drawn as the black dash dot line in Fig. 4, is in great accordance with experiment values. Thus, we believe that the anharmonic calculations such as the phonon scattering rates are accurate enough. The isotropic thermal conductivity for natural wurtzite GaN at room temperature is obtained to be 239.26 W/mK.

The discrepancy of thermal conductivity in [0001] and [01$\bar{1}$0] directions calculated from the first principle is listed in Table I. The discrepancy increases with decreasing temperature and the anisotropy of natural GaN is more significant than that of the isotopically pure GaN. The discrepancy reaches 40.08% for natural GaN at 100 K and the temperature influence on the anisotropy of natural GaN is larger than that of pure GaN.

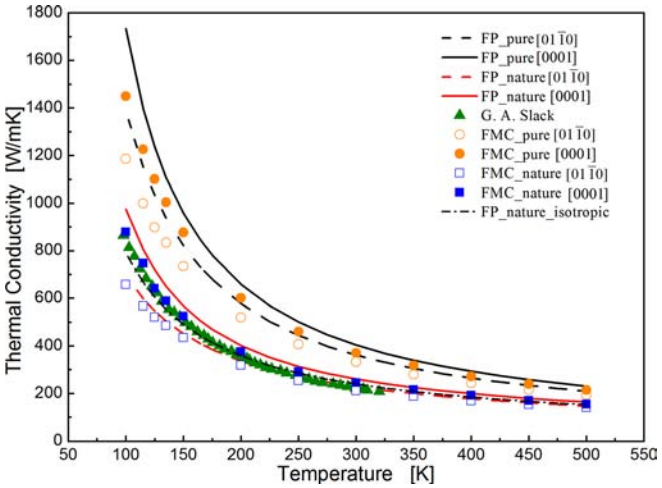

FIG. 4. The calculated thermal conductivity of the wurtzite GaN bulk material. The dash lines and solid lines are first principle calculations for lattice direction [01$\bar{1}$0] and [0001], respectively. The hollow symbols and solid symbols are Monte Carlo calculations for lattice direction [01$\bar{1}$0] and [0001], respectively. The solid triangles represent experiment values from Slack *et al*. The black dash dot line is the isotropic thermal conductivity for natural GaN.

The calculated thermal conductivity of pure and natural bulk GaN from the FMC method is shown in Fig. 4, which are in agreement with both experiment data and the first principle values within the margin of error. These results validated our FMC method. Thermal conductivity can be determined by the temperature difference and the heat flux through the medium according to the Fourier's law. And the heat flux along the temperature gradient should be calculated according to[23]

$$q = \frac{1}{V_{all}} \sum_{i=1}^{N} e_i \langle \vec{v}_g(i) \cdot \vec{k} \rangle, \tag{9}$$

where e_i is the phonon energy, $\langle \vec{v}_g(i) \cdot \vec{k} \rangle$ represents the velocity along the temperature gradient, V_{all} is the volume of the model, and N is the number of phonons. Thermal conductivities obtained by the FMC method are a little lower than the corresponding first principle results, due to the fact that the former method solves the BTE by relaxation time approximation while the latter one by iteration. Values of k_x and k_z obtained by the FMC method for natural GaN at 300 K are 211.36 W/mK and 244.81 W/mK.

To study the anisotropy in GaN, the frequency dependent thermal conductivity contribution for pure and natural bulk GaN at various temperatures is shown in Fig. 5. We define the frequency between 0–4 THz, 4–7.74 THz, and 7.74–22.12 THz to be low-, medium-, and high-frequency, respectively, just for convenience. The contribution of medium-frequency phonons to thermal conductivity is significant especially at high temperatures, which has the percentage of 62.01% and 43.06% at 300 K for pure GaN and natural GaN, respectively. With the temperature decreasing, low-frequency phonons contribute more, making the anisotropy stronger, owing to the large discrepancy of the phonon group velocity in the low-frequency region between [01$\bar{1}$0] and [0001] directions.[32] Comparing Fig. 5(a) with Fig. 5(b), we found that the contribution of medium-frequency phonons is weakened by isotopic scatterings, so that the low-frequency phonons contribute relatively more in natural GaN, resulting in stronger anisotropy. From Fig. 5(c), we can see that the isotopic scattering rate is quite large in the medium-frequency region (see the green rectangle), and is even larger than the intrinsic scattering rate to the extent that the isotopic scattering process becomes dominant. Thereby, the phonon MFP of medium-frequency phonons shown in Fig. 5(d) is remarkably weakened by the isotropic scattering process, resulting in lower thermal conductivity. In spite that the direct contribution of optical phonons with higher frequencies is extremely small, scattering rates of optical phonons are large, so that there are more possibilities for high-frequency phonons to change into lower-frequency phonons.

B. Out-of-plane of GaN thin film

Phonon transport in the wurtzite GaN thin film is simulated based on the model as showed in Fig. 3. The upper surface and the lower surface are isothermal boundaries with temperature difference, so that the thermal conductivities in the out-of-plane direction for *C*-mode and *A*-mode are calculated. The out-of-plane direction is defined along the film thickness direction. Results are shown in Fig. 6 and the values are much smaller than the bulk condition. The thermal conductivity in the out-of plane direction with film thickness of 50 nm for the *C*-mode at 300 K is only 33.84 W/mK. The thermal conductivity in this work is the overall equivalent thermal conductivity calculated by the Fourier's law. Fig. 6(b) shows that $1/k$ is not linear with $1/L$ resulting in that the approach to predict the thermal conductivity of bulk GaN by linear extrapolation of $1/k$ vs. $1/L$ to the $1/L \rightarrow 0$ limit is not available. This was also found by Liang *et al*. using the non-equilibrium molecular dynamic method.[33] Results in Fig. 6(a) indicate that the anisotropy is reduced with decreasing film thickness and even disappear when the size effect is very strong. Therefore, changing the lattice direction in the wurtzite GaN thin film has little effect on the out-of-plane thermal transport.

TABLE I. The discrepancy of thermal conductivities of x and z direction.

Temperature (K)	100	150	200	250	300	350	400	450	500
k_x_pure (W/mK)	1387.12	821.56	577.94	444.55	361.64	305.28	264.45	233.45	209.07
k_z_pure (W/mK)	1733.64	959.07	658.54	500.42	404.14	339.56	293.19	258.22	230.86
Discrepancy (%)	24.98	16.74	13.95	12.57	11.75	11.23	10.87	10.61	10.42
k_x_natural (W/mK)	696.51	451.96	336.48	270.55	228.56	199.38	177.75	160.92	147.37
k_z_natural (W/mK)	975.68	567.99	401.35	313.78	260.67	224.98	199.13	179.37	163.66
Discrepancy (%)	40.08	25.67	19.28	15.98	14.05	12.84	12.03	11.46	11.06

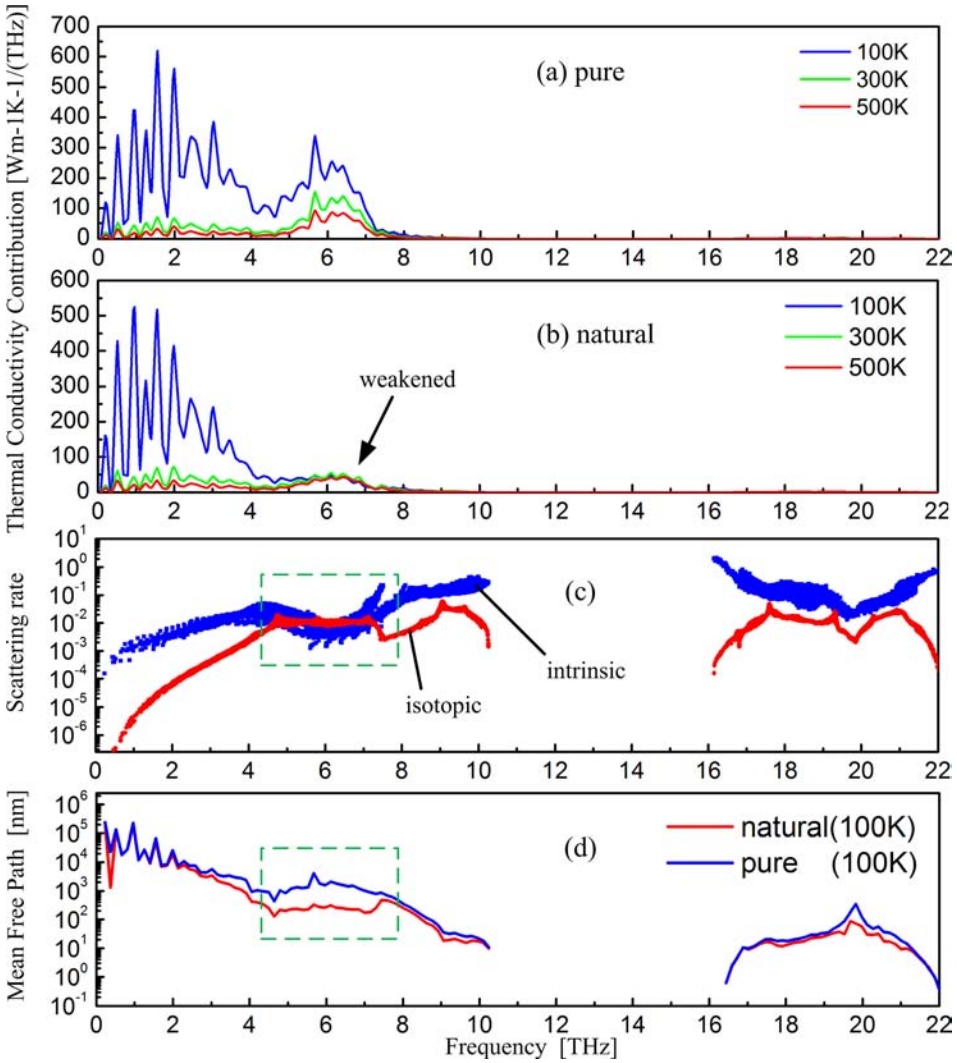

FIG. 5. Frequency dependent properties of (a) thermal conductivity contribution for pure GaN; (b) thermal conductivity contribution for natural GaN; (c) scattering rates of intrinsic and isotopic scattering processes; (d) the phonon mean free path of natural and pure GaN at 100 K.

Fig. 7 shows the frequency dependent thermal conductivity contribution of various film thicknesses at 300 K. When decreasing the film thickness, the contribution of both low-frequency and medium-frequency phonons decreases. However, the low-frequency phonons, which have long phonon mean free paths, are impacted by the size effect more heavily, so that the peak in the low-frequency region disappears when the film thickness reduces to 50 nm. As low- and medium-frequency phonons are confined, the contribution of high-frequency phonons is nearly independent from size effect. Their contribution becomes larger with the thickness decreased; thus, they would better be taken into account when the size effect is strong. Isotopic scattering processes effect mostly on medium-frequency phonons. However, the low-frequency phonons are not influenced owing to their large mean free paths and low isotopic scattering rates. As a result, low-frequency phonons may travel across the film by ballistic transport without intrinsic and isotopic scattering events and reach the isothermal boundary resulting in strong confinements.

Fig. 8 shows the frequency dependent normalized cumulative function of the thermal conductivity contribution.

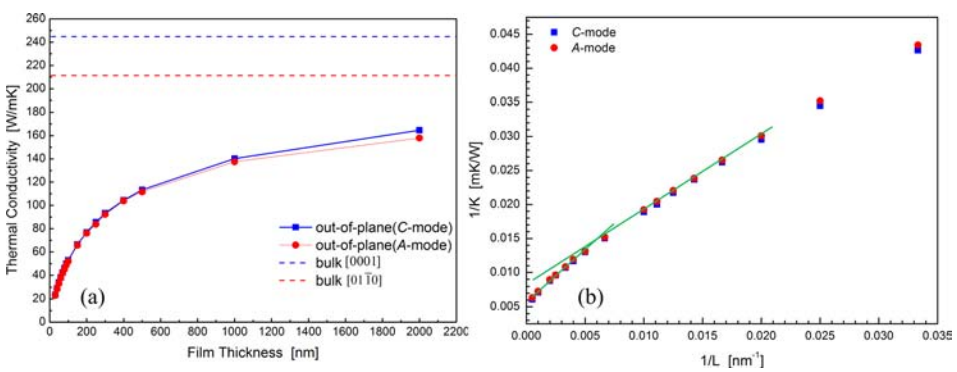

FIG. 6. (a) The curves of the out-of plane thermal conductivity of natural GaN thin films at 300 K changing with the thin film thickness. The up-limits are calculated in bulk condition. (b) The out-of-plane $1/k$ vs. $1/L$ for natural wurtzite GaN thin films both in *C*-mode and *A*-mode at 300 K. Two green straight lines are the schematic linear fits of partial data points of $1/k$ vs. $1/L$.

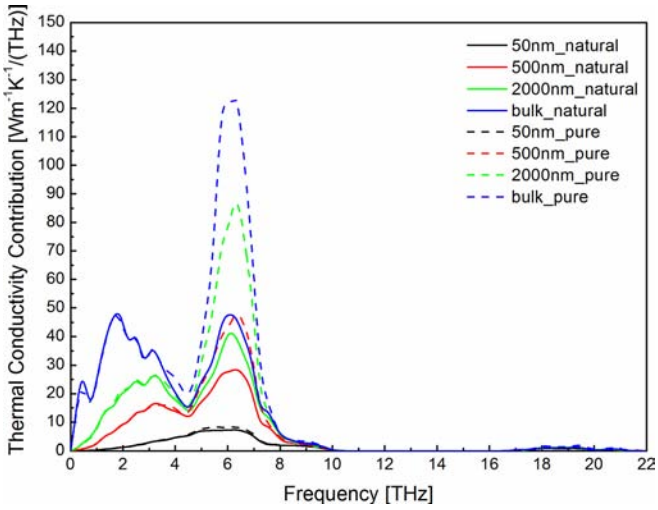

FIG. 7. Frequency dependent out-of plane thermal conductivity contribution of various film thicknesses for pure and natural wurtzite GaN at 300 K.

Results indicate that the ratio of low-frequency phonons' contribution to the overall thermal conductivity gets smaller when thin film thickness is decreased. Thereby, the low-frequency part with significant anisotropy is less important, leading to smaller anisotropy in thermal conductivity. In result, size effect in the temperature gradient direction strongly confined the anisotropy.

C. In-plane of GaN thin film

The thermal conductivity of the in-plane direction, which is defined as the direction normal to the film thickness, is calculated by transforming the boundary conditions in the FMC method. The left and right boundaries are set to be isothermal with temperature difference using the periodic boundary condition, so that the heat transfer is normal to the film thickness. The degrees of specularity d of the front and back boundaries are assigned to be unit. There is a negative correlation between the specularity and the surface roughness which is determined through the relation[34,35]

$$d = \exp\left(-\frac{16\pi^3\eta^2}{\lambda^2}\right), \tag{10}$$

where λ is the phonon wavelength and η is the average surface roughness.

We changed the specularity d from zero to unit and obtained the in-plane thermal conductivity of the natural wurtzite GaN thin film with thickness of 50 nm, as shown in Fig. 9. Results indicate that the in-plane thermal conductivity reduces due to stronger phonon-boundary interactions when the surface roughness increases. It was also observed that large anisotropy exists in the in-plane thermal conductivity. With the specularity reduced, the thermal conductivity discrepancies remain nearly unchanged in the result of increased anisotropy. The A-mode in-plane thermal conductivity becomes 35.63% larger than that of the C-mode with the specularity of zero, with the value of 112.214 W/mK and 82.736 W/mK for the former and latter, respectively. Thus, the film surface roughness enhances the anisotropy of the wurtzite GaN thin film.

To figure out the reason why this phenomenon happens, we calculated the temperature gradient along the in-plane direction in the wurtzite GaN thin film with thickness of 50 nm at 300 K for various degrees of specularity d. The calculation domain is divided into five regions and the temperature of each region can be obtained. Fig. 10 shows the results. The temperature profiles are approximately linear indicating that phonons transport diffusively along the in-plane direction, without ballistic transports caused by the size effect. Therefore, intrinsic scattering process plays an important role in the in-plane phonon transport in the GaN thin film at room temperature. This is totally different from the phonon transport along the out-of-plane direction when large temperature discrepancy exists at the isothermal boundary caused by the ballistic phonon transport. Besides, the boundary interaction only changes the direction of phonons' group velocity, so the phonon confinement is extremely weak. Thus, the anisotropy should be nearly the same with the corresponding bulk condition if the effect of the

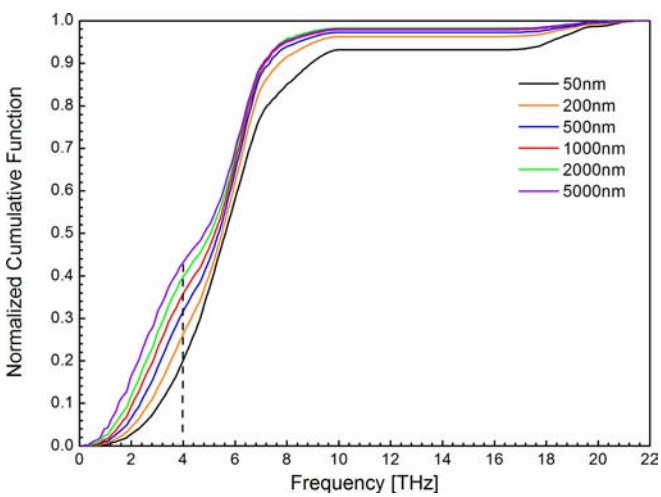

FIG. 8. Frequency dependent normalized cumulative function of the thermal conductivity contribution of different thin film thicknesses calculated for natural wurtzite GaN at 300 K.

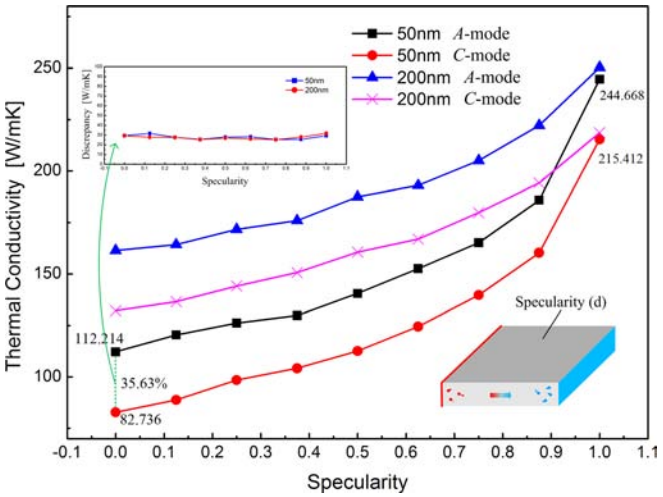

FIG. 9. The in-plane thermal conductivity of the natural wurtzite GaN thin film with thickness of 50 nm at 300 K vs. specularity for C-mode and A-mode. Inset: the discrepancies between the in-plane thermal conductivity of C-mode and A-mode.

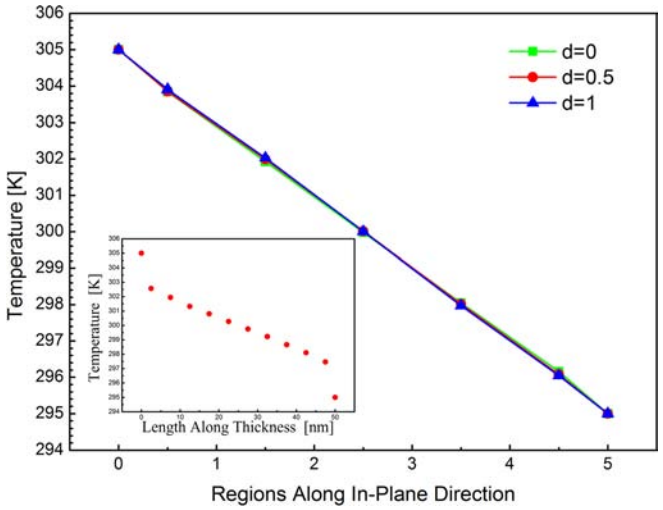

FIG. 10. Temperature profiles along the in-plane direction in the GaN thin film with thickness of 50 nm at 300 K for various degrees of specularity d. Inset: the temperature profile along the out-of-plane direction in the GaN thin film with thickness of 500 nm at 300 K.

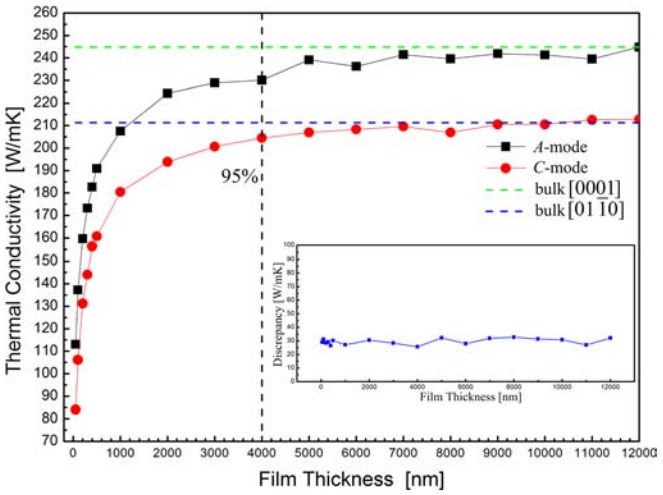

FIG. 12. The in-plane thermal conductivity of the natural wurtzite GaN thin film with d = 0 at 300 K for C-mode and A-mode as a function of the film thickness. The green and blue dash lines are the up-limit calculated under the bulk condition both for [0001] and [01$\bar{1}$0] directions, respectively. Inset: the discrepancies between the in-plane thermal conductivity of C-mode and A-mode.

boundary interactions for the C-thick mode and A-thick mode are the same. However, we can see in Fig. 11 that the phonon group velocity of low frequency phonons in the [0001] direction is obviously larger than that in the [01$\bar{1}$0] direction. The larger group velocity component of the film thickness direction leads to more boundary interactions.[9] Therefore, the boundary effect of the A-mode should be stronger than that of the C-mode. The decreasing of the degree of specularity d also increases the boundary scattering rates, which strengthened the boundary effect difference between the C-mode and the A-mode. Thus, the anisotropy increases with d decreased.

Fig. 12 shows the in-plane thermal conductivity as a function of the film thickness. The similar phenomenon is observed since the decreasing of the film thickness only strengthened the boundary interaction which is similar to the decreasing of the degree of specularity. With the film thickness decreased, the anisotropy of thermal conductivity increases. The finite size effect in the in-plane direction is much weaker than the strong size effect in the out-of-plane direction. The thermal conductivity reaches 95% of the corresponding bulk thermal conductivity when the film thickness reduced to 4 μm.

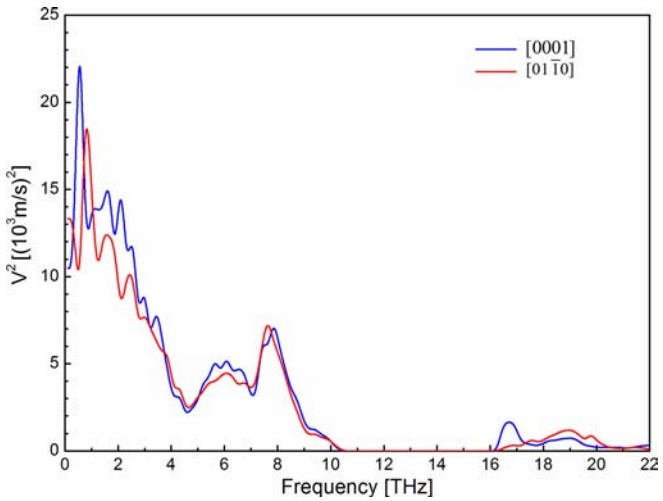

FIG. 11. The average of the square of group velocities along [0001] and [01$\bar{1}$0] directions calculated in bulk GaN material at 300 calculated using the FMC method.

IV. CONCLUSIONS

We developed a first-principle-based FMC simulation method to study the anisotropic phonon transport in the wurtzite GaN thin film. The first principle method is implemented to obtain the thermal properties of the bulk wurtzite GaN as the input data of the FMC method. All the phonon modes are considered and the scattering rates are obtained without involving any empirical parameters in the FMC method. We calculated the thermal conductivity as a function of temperature for the natural and pure GaN in good agreement with the first principle results as well as the experimental data. It is observed that the anisotropy of the thermal conductivity increases with the temperature decreasing and it is strengthened by isotopic scatterings due to relatively more contribution of the low-frequency phonons which have the anisotropic phonon group velocity. With the decreasing of the GaN thin film thickness, the out-of-plane thermal conductivity reduces to 33.84 W/mK and the anisotropy is also weakened due to less importance of the low-frequency phonons and the strong size effect caused by the ballistic phonon transport. On the contrary, with the film thickness reduced, the anisotropy of the in-plane thermal conductivity is strengthened caused by heavier boundary interactions. The in-plane thermal conductivities of the A-mode and C-mode for the wurtzite natural GaN thin film with thickness of 50 nm at 300 K are 112.214 W/mK and 82.736 W/mK, respectively, leading to the anisotropy value of 35.63%. Thus, the lattice direction in the GaN thin film has great effect on the in-plane thermal conductivity while it has little effect on the out-of-plane thermal conductivity. Besides,

the size effect in the out-of-plane direction is much smaller, so that the out-of-plane thermal conductivity is still 95% of the bulk situation when the film thickness reduced to 4 μm. What more, the anisotropy of the in-plane thermal conductivity is also strengthened by increasing the surface roughness of the GaN thin film.

ACKNOWLEDGMENTS

The financial support by the National Natural Science Foundation of China (Grants Nos. 51576078, 51376070), and the 973 Project of The Ministry of Science and Technology of China (Grant No. 2011CB013105) are acknowledged. The authors would like to acknowledge the fruitful discussion with Mr. Ma Jinlong from Huazhong University of Science and Technology.

[1]Q. Shan, Q. Dai, S. Chhajed, J. Cho, and E. F. Schubert, J. Appl. Phys. **108**, 084504 (2010).
[2]T. Wang, J. Xu, and X. Wang, Chin. Sci. Bull. **57**(30), 3937–3942 (2012).
[3]I. A. Prudaev, V. V. Kopyev, I. S. Romanov, and V. N. Brudnyi, Russ. Phys. J. **58**(5), 641–645 (2015).
[4]S. J. Wang, K. M. Uang, S. L. Chen, Y. C. Yang, S. C. Chang, T. M. Chen, and C. H. Chen, Appl. Phys. Lett. **87**, 011111 (2005).
[5]J. C. Johnson, H. J. Choi, K. P. Knutsen, R. D. Schaller, P. D. Yang, and R. J. Saykally, Nat. Mater. **1**, 106 (2002).
[6]Z. Su, L. Huang, F. Liu, J. P. Freedman, L. M. Porter, R. F. Daves, and J. A. Malen, Appl. Phys. Lett. **100**, 201106 (2012).
[7]B. A. Danilchenko, T. Paszkiewicz, S. Wolski, A. Jezowski, and T. Plackowski, Appl. Phys. Lett. **89**, 061901 (2006).
[8]D. Lacroix, K. Joulain, and D. Lemonnier, Phys. Rev. B **72**, 064305 (2005).
[9]D. Lacroix, K. Joulain, D. Terris, and D. Lemonnier, Appl. Phys. Lett. **89**, 103104 (2006).
[10]M. S. Jeng, R. Yang, D. Song, and G. Chen, J. Heat Transfer **130**, 042410 (2008).
[11]Q. Hao, G. Chen, and M. S. Jeng, J. Appl. Phys. **106**, 114321 (2009).
[12]B. T. Wong, M. Francoeur, and M. P. Menguc, Int. J. Heat. Mass. Transfer **54**, 1825–1838 (2011).
[13]J. P. M. Peraud and N. G. Hadjiconstantinou, Appl. Phys. Lett. **101**, 153114 (2012).
[14]V. Jean, S. Fumeron, K. Termentzidis, X. Zianni, and D. Lacroix, Int. J. Heat. Mass. Transfer **86**, 648–655 (2015).
[15]S. Mazumder and A. Majumdar, J. Heat Transfer **123**, 749 (2001).
[16]C. Kittel, *Introduction to Solid State Physics*, 6th ed. (John Wiley & Sons Inc., 1986).
[17]P. G. Klemens, "Thermal conductivity and lattice vibrational modes," in *Solid State Physics*, edited by F. Seitz and D. Turnball (Academic Press, NY, 1958), Vol. 7.
[18]S. Mei, L. N. Maurer, Z. Aksamija, and I. Knezevic, J. Appl. Phys. **116**, 164307 (2014).
[19]J. Garg, Ph.D. thesis, Massachusetts Institute of Technology, 2011.
[20]L. Lindsay, D. A. Broido, and T. L. Reinecke, Phys. Rev. Lett. **109**, 095901 (2012).
[21]C. Mion, J. F. Muth, E. A. Preble, and D. Hanser, Appl. Phys. Lett. **89**, 092123 (2006).
[22]J. Philippe, M. Peraud, and N. G. Hadjiconstantinou, Phys. Rev. B **84**, 205331 (2011).
[23]J. Ma, X. Wang, B. Huang, and X. Luo, J. Appl. Phys. **114**, 074311 (2013).
[24]A. Mittal and S. Mazumcer, J. Heat. Transfer **132**, 052402 (2010).
[25]W. Li, J. Carrete, N. A. Katcho, and N. Mingo, Comput. Phys. Commun. **185**, 1747 (2014).
[26]S. Baroni *et al*., See http://www.quantum-espresso.org for more information about the QUANTUM ESPRESSO package.
[27]T. Ruf, J. Serrano, and M. Cardona, Phys. Rev. Lett. **86**, 906 (2001).
[28]H. Schulz and K. H. Thiemann, Solid State Commun. **23**, 815 (1977).
[29]J. M. Zhang, T. Ruf, and M. Cardona, Phys. Rev. B **56**(22), 14399 (1997).
[30]N. W. Ashcroft and N. D. Mermin, *Solid State Physics* (Saunders College, Philadelphia, 1976).
[31]G. A. Slack, L. J. Schowalter, D. Morelli, and J. A. Freitas, J. Cryst. Growth **246**, 287 (2002).
[32]J. Ma, W. Li, and X. Luo, Appl. Phys. Lett. **105**, 082103 (2014).
[33]Z. Liang, A. Jain, A. J. H. McGaughey, and P. Keblinski, J. Appl. Phys. **118**, 125104 (2015).
[34]J. M. Ziman, *Electrons and Phonons: The Theory of Transport Phenomena in Solids* (Oxford, Clarendon Press, 1960).
[35]X. Wang and B. Huang, Sci. Rep. **4**, 6399 (2014).